$EuMn_2Ge_2$ and $EuMn_2Si_2$: Magnetic structures and valence transitions

M. Hofmann,[1,*] S. J. Campbell,[2,1] and A. V. J. Edge[2]
[1]*Technische Universität München, FRM II, Lichtenbergerstr 1, D-85747 Garching, Germany*
[2]*School of Physical, Environmental and Mathematical Sciences, The University of New South Wales, Australian Defence Force Academy, Canberra, ACT 2600, Australia*
(Received 28 January 2004; published 28 May 2004)

The magnetic structures of $^{153}EuMn_2Ge_2$ and $^{153}EuMn_2Si_2$ have been determined by neutron diffraction measurements ($\sim$1.8–723 K). The Mn sublattices of both $EuMn_2Ge_2$ and $EuMn_2Si_2$ order antiferromagnetically [$T_N = 667(9)$ K; space group $I4'/m'm'm$ and $T_N = 391(5)$ K; space group $I_p4/m'm'm'$, respectively] with no evidence for ordering of the Eu^{+2} ions in $EuMn_2Ge_2$ down to 1.5 K. $EuMn_2Si_2$ exhibits a thermally driven valence transition around $T_v \sim 527$ K with a pronounced increase in the unit cell volume of $\sim$7% from the Eu^{3+} state at low temperatures ($T < \sim 150$ K) to an average valence state of $\sim$2.5 at high temperatures ($T > \sim 600$ K). The valence-induced volume changes have been analyzed for the first time in terms of the interconfigurational fluctuation model with occupation probabilities for the Eu^{2+} state in $EuMn_2Si_2$ and the average Eu^{val} values found to agree well with our reanalysis of earlier $^{151}EuMn_2Si_2$ isomer shift data. The strength of the magnetic interaction for antiferromagnetic ordering of the Mn sublattice is decreased by $\sim$10%–15% as a result of the change in the electronic configuration of $EuMn_2Si_2$.

DOI: 10.1103/PhysRevB.69.174432 PACS number(s): 75.25.+z, 87.64.Bx, 75.20.Hr

I. INTRODUCTION

Interest in characterizing and understanding the behavior of intermediate valence systems of the $4f$ electron series has continued unabated for several decades (e.g., Refs. 1–3). Rare-earth (R) intermetallic compounds containing europium are of special interest—they exhibit a wide range of unusual physical and magnetic properties as well as intermediate valences associated with the transition from the Eu^{2+} ($4f^6$) configuration to the Eu^{3+} ($4f^7$) configuration (e.g., Ref. 4). Ternary EuT_2M_2 compounds (T = transition metal; M = Si, Ge, P) with the tetragonal $ThCr_2Si_2$-type structure have attracted particular attention as the pure 1-2-2 compounds form readily and solid solutions can also be formed across wide concentration ranges of the T and M elements. This enables aspects of valence transitions linked with substitutional effects in pseudoternary systems to be investigated (e.g., Refs. 5–8), in addition to the intrinsic behavior of the valence transitions in the pure 1-2-2 compounds themselves. An additional feature is the influence of the transition metal to the overall magnetism of the compounds. For example, the Ni sublattice in $EuNi_2Si_{2-x}Ge_x$ is nonmagnetic,[5,8] whereas the Mn sublattice exhibits magnetic order in $EuMn_2Si_{2-x}Ge_x$[6] as indeed it does in all $RMn_2Si_{2-x}Ge_2$ compounds (e.g., Refs. 4, 9).

The temperature-induced valence transitions in EuT_2M_2 systems have been investigated by a variety of techniques, including ^{57}Fe[6] and ^{151}Eu Mössbauer spectroscopy,[5,6] x-ray absorption spectroscopy,[5,8] as well as x-ray diffraction, magnetic susceptibility, magnetization, and resistivity measurements.[5,6,8,10] Changes in the valence state induced by applied pressure[11,12] and magnetic field[8] have also been investigated in Eu-based compounds. While the main factors governing the magnetic ordering and structures of most RM_2M_2 compounds are well documented (e.g., Refs. 4, 9, 13), the magnetic structures of $EuMn_2M_2$ compounds are less well understood; this is due mainly to the large neutron absorption of natural Eu (e.g., 4530 b at a neutron energy of 25.3 meV). In the case of $EuMn_2Si_{2-x}Ge_x$, Nowik *et al.*[6] have recently reported that $EuMn_2Ge_2$ contains divalent Eu and that large changes in the Eu valence and the magnetism of the Mn sublattice are caused on replacing Ge with Si, while $EuMn_2Si_2$ reveals features consistent with a transformation from Eu^{3+} to Eu^{2+} above $\sim$500 K. They report that the Mn sublattice orders antiferromagnetically for both $EuMn_2Ge_2$ and $EuMn_2Si_2$—the former as a canted antiferromagnet and the latter with spin reorientations also occurring.

Given the range of valence and magnetic effects taking place in this system, we have carried out neutron diffraction measurements on $^{153}EuMn_2Si_2$ and $^{153}EuMn_2Ge_2$ in order to clarify the unresolved issues concerning the magnetic and valence behavior of those compounds. We have determined the hitherto unknown magnetic structures of $EuMn_2Ge_2$ and $EuMn_2Si_2$ and analyzed the anomalous volume changes observed in $EuMn_2Si_2$ above ambient temperature by an extension of the interconfigurational fluctuation model in which the rare earth ions can be described as fluctuating in time between two configurations and in which the effect of cooperative phenomena in concentrated Eu compounds are taken into account.[14,15] Good agreement is found between the occupation probability determined for the Eu^{2+} state of $^{153}EuMn_2Si_2$ from the present analysis of volume change data and our reanalysis of earlier $^{151}EuMn_2Si_2$ isomer shift data.

II. EXPERIMENTAL

The neutron diffraction measurements were carried out on the time-of-flight diffractometer GEM ($\sim$7–723 K) at the ISIS spallation neutron source, UK. Additional measurements were carried out on the $EuMn_2Ge_2$ sample on the E6 diffractometer ($\sim$1.8–300 K; wavelength $\lambda = 2.444$ Å) at the Hahn–Meitner Institut, Germany. An important feature of these experiments was the investigation of compounds using

the low neutron absorption isotope ^{153}Eu (of natural abundance ~52.2%) as the large absorption cross section of the ^{151}Eu isotope prohibited the use of samples prepared with natural Eu. The ^{153}Eu was purchased in the form of a ~0.5 g metallic sheet of purity ~99.9% and of enrichment 98.77% in the ^{153}Eu isotope (Oak Ridge National Laboratory) with the 99.999% Si, 99.999% Ge, and 99.99% Mn purchased from Aldrich Chemicals, RIC Corporation, and Goodfellow, respectively. While standard preparation techniques were used, in view of the high cost of the ^{153}Eu isotope, particular care was taken in the preparation of the ~0.5 g $^{153}EuMn_2Ge_2$ and $^{153}EuMn_2Si_2$ samples. Samples of equivalent mass were initially prepared using natural Eu to refine the preparation technique. In view of the highly pyrophoric reactivity of Eu, the starting materials were handled in an argon gas chamber. Ultimately, samples were prepared in a standard argon arc furnace with each sample remelted up to seven times. The ingot was weighed after each separate melt and the melting process completed when the target mass—corresponding to the stoichiometry of the 1-2-2 compounds—was reached. Before the initial melt, 17.5% excess ^{153}Eu and 3.5% excess Mn were added to compensate for evaporative losses during the argon arc melts.

The experiments on GEM were carried out over the temperature ranges ~7–723 K for $EuMn_2Si_2$ and ~7–650 K for $EuMn_2Ge_2$ using a standard cryofurnace. The samples were mounted in thin-walled vanadium cans of diameter 3 mm in order to further reduce the neutron absorption effects. The E6 experiments on $EuMn_2Ge_2$ covered the temperature range ~1.8–300 K and the sample was mounted in a thin Al cylinder (diameter 2 mm). In this form the final samples had an absorption cross section of ~342 b at a neutron energy of 25.3 meV compared with a cross section of ~4380 b for the equivalent samples prepared with natural Eu. The crystal and magnetic structures were determined from the diffraction patterns by Rietveld refinements using the computer program GSAS.[16] This allowed the data from the four available detector banks of GEM[17]—each covering a different *d*-spacing range—to be refined simultaneously. X-ray diffraction patterns confirmed that both samples crystallize in the $ThCr_2Si_2$-type structure, as expected. In conjunction with the neutron diffraction measurements, it is estimated that small-level impurity phases are present in both samples. For example, ~2%–3% EuO is present in $^{153}EuMn_2Si_2$ with ~2%–3% EuO present in $^{153}EuMn_2Ge_2$. Given the low level of these impurity phases and the need to simultaneously refine the crystal and magnetic structures, these phases were not included in the Rietveld refinements.

III. RESULTS AND DISCUSSION

As described below, $^{153}EuMn_2Ge_2$ was found to exhibit more straightforward structural and magnetic behavior compared with $^{153}EuMn_2Si_2$. We therefore consider the results and analysis of the $^{153}EuMn_2Ge_2$ sample first in the discussion.

A. $^{153}EuMn_2Ge_2$: Magnetic structure

Figure 1 shows the neutron diffraction patterns of $^{153}EuMn_2Ge_2$ from two different detector banks of GEM at 398 K along with Rietveld refinements to the data. The refinements in Figs. 1(a) and 1(b) represent the fit obtained solely on the basis of the $ThCr_2Si_2$-type structure appropriate to this class of 1-2-2 compound. The misfit to the data is evident, indicating the presence of significant magnetic scattering in $^{153}EuMn_2Ge_2$ at 398 K. By comparison, the refinements in Figs. 1(c) and 1(d) represent the high quality fit ($\chi^2 \sim 2.4$) obtained based on the antiferromagnetic structure for $^{153}EuMn_2Ge_2$ described below.

As outlined previously,[18] for the RMn_2X_2 series with the $ThCr_2Si_2$-type structure, a ferromagnetic order of the Mn sublattice would lead to an increase in the intensity of peaks obeying the reflection conditions $h+k=2n$. However, as indicated by Fig. 1, for $^{153}EuMn_2Ge_2$, we find that the intensities of several reflections [e.g., (101), (103), (105)] are enhanced compared with the nuclear scattering expected from the 1-2-2 lattice. The occurrence of magnetic intensity in such peaks with $h+k=2n+1$ satisfies the reflection conditions for an anti-*c*-lattice translation mode. This leads to the result that Mn atoms at the (0, 1/2, 1/4) and (1/2, 0, 1/4) positions have magnetic moments pointing in the opposite direction to each other. Further, as discussed fully elsewhere e.g., Refs. 18, 19, the intensity ratio for the (101) and (103) peaks indicates that the moment direction is along the *c* axis rather than in the (110) plane. The variation of the intensity of the (101) magnetic peak with temperature is shown in Fig. 2(a) with the variations of the nuclear (200) and (110) reflections shown for comparison. The magnetic structure of $EuMn_2Ge_2$, space group $I4'/m'm'm$, is depicted in Fig. 2(b).

The lattice parameters of $EuMn_2Ge_2$ at ambient temperature [$a=4.249\,72(3)$ Å; $c=10.9084(2)$ Å from the present investigation] correspond well with the values for $SrMn_2Ge_2$ ($a=4.30$ Å; $c=10.91$ Å).[20] Given the further similarity in the ionic radii of Sr^{2+} ($r=1.32$ Å) and Eu^{2+} ($r=1.31$ Å),[21] this equivalence in structural parameters between $SrMn_2Ge_2$ and $EuMn_2Ge_2$ provides clear evidence that Eu ions are in the Eu^{2+} valence state in $EuMn_2Ge_2$, in agreement with earlier findings (e.g., Ref. 6). The arrangement of magnetic moments on the Mn sublattice shown in Fig. 2(b) is similar to the magnetic structure found in the earth alkaline intermetallic compounds $CaMn_2Ge_2$ and $BaMn_2Ge_2$.[19] In light of the common 2+ valence state for the $CaMn_2Ge_2$, $BaMn_2Ge_2$, and $EuMn_2Ge_2$ compounds and given the small magnetization for $EuMn_2Ge_2$,[22] Malaman *et al.*[19] noted the possibility of antiferromagnetic (001) Mn layers in $EuMn_2Ge_2$, as established in the present experiments.

The Néel temperature of $EuMn_2Ge_2$ is above the highest temperature, 623 K, accessible to us within the limited time available for our experiments. Nonetheless, as shown in Fig. 2(b), by fitting the refined magnetic moment values to the expression $\mu(T)=\mu(0)[1-(T/T_N)^d]^e$,[23] a value of $T_N=667(9)$ K is obtained with $\mu(0)=3.43(4)\ \mu_B$ and fit parameters $d=2.7(3)$ and $e=0.36(3)$. This expression was chosen as a convenient empirical function to represent the

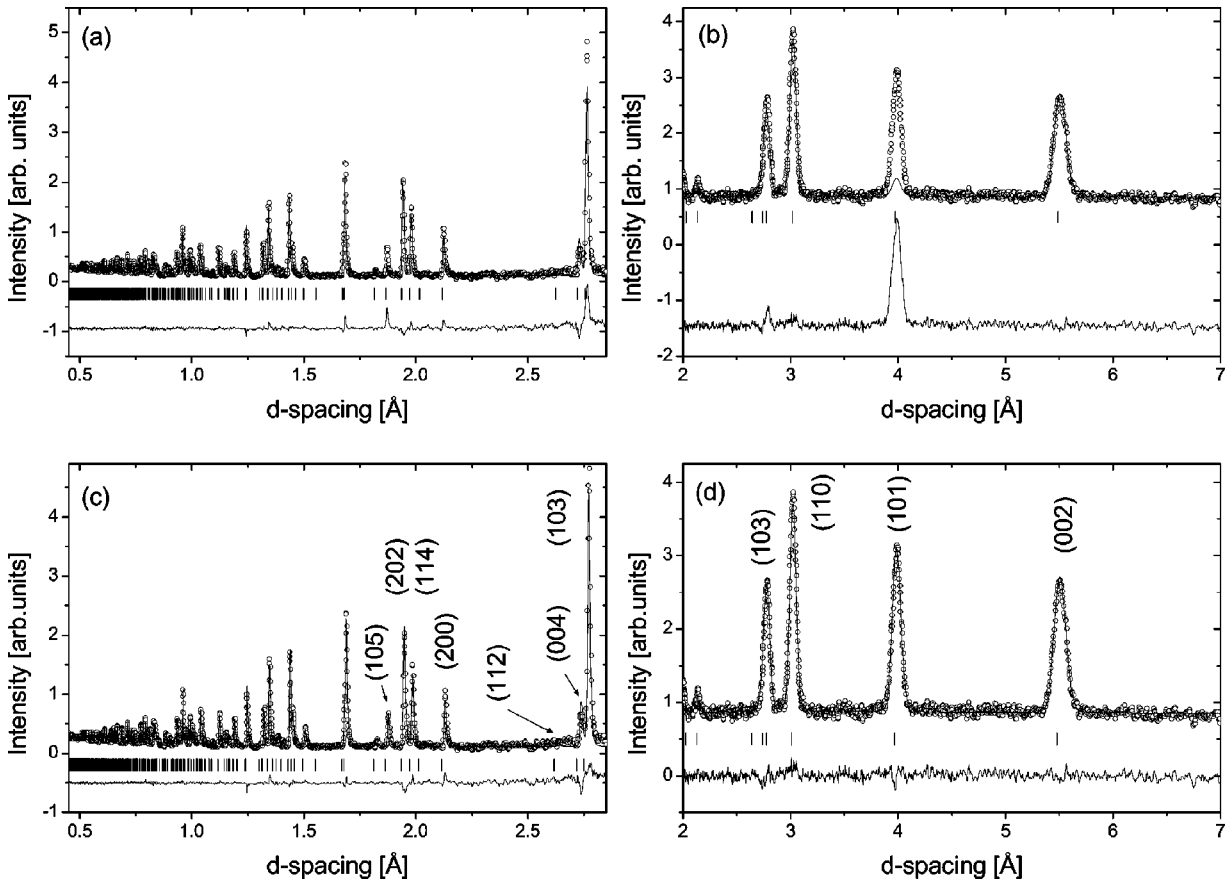

FIG. 1. Rietveld refinements to the time of flight neutron powder diffraction patterns of $^{153}EuMn_2Ge_2$ at 398 K. Diffraction patterns are shown for the 17° bank (a) and the 90° bank (b) of the diffractometer GEM, ISIS with the patterns repeated in Figs. 1(c) and 1(d). The refinement in (a) and (b) represents the fit to the $ThCr_2Si_2$-type structure and is intended to draw out the magnetic scattering in $^{153}EuMn_2Ge_2$ at this temperature. The refinements in (c) and (d) represent the refinement to the axial antiferromagnetic structure for $^{153}EuMn_2Ge_2$ [Fig. 2(b)], as described in the text.

trends of the data. The refined magnetic moment on the Mn atoms was determined to be $\mu_{Mn}=3.41(7)\ \mu_B$ at 1.8 K. This relatively high value for the Mn moment in $EuMn_2Ge_2$ compared with that typically found in such $ThCr_2Si_2$-type compounds, is consistent with the values of $2.67(5)\ \mu_B$ and $3.66(3)\ \mu_B$ found for $CaMn_2Ge_2$ and $BaMn_2Ge_2$, respectively, at 2 K.[19] This behavior can be correlated with the Mn–Ge distances and the nature of this bond.[24]

The present findings disagree with earlier magnetization and Mössbauer effect measurements that claim antiferromagnetic order for the Mn sublattice below a first-order transition temperature $T_N\sim 302$ K.[6] As indicated above, the present results demonstrate clearly the occurrence of antiferromagnetic scattering at 398 K (Fig. 1), which persists to the continuous magnetic transition at $T_N=667(9)$ K (Fig. 2). The possibility of observing magnetic ordering of the Eu^{2+} ions in the present neutron experiments was also of strong interest. Based on their magnetization measurements, Nowik *et al.*[6,22] reported ferromagnetic ordering of the Eu^{2+} ions below a transition temperature of $T_C\sim 13$ K. By comparison, in the present set of eight neutron diffraction measurements from 30 to 1.8 K, no evidence, either by way of enhancement in the scattering at nuclear peak positions [see Fig. 2(b)] or by the occurrence of additional magnetic peaks, was obtained for magnetic ordering of Eu in $EuMn_2Ge_2$ down to $T=1.8$ K. The small fraction (~2%–3%) of EuO (ferromagnetic with $T_c\sim 76$ K[25]) detected from the neutron diffraction patterns of our $^{153}EuMn_2Ge_2$ sample did not influence the crystallographic or magnetic structural refinements of the 1-2-2 phase. On the other hand, small fractions of strongly magnetic impurity phases can contribute disproportionately to the magnetization measurements of weakly magnetic systems. In summary, it is concluded that $EuMn_2Ge_2$ exhibits collinear antiferromagnetism below a Néel temperature of $T_N=667(9)$ K rather than canted antiferromagnetism with a first-order transition at $T_N=302$ K, as proposed previously.[6]

B. $^{153}EuMn_2Si_2$: Magnetic structure

Figure 3 shows the neutron diffraction patterns of $^{153}EuMn_2Si_2$ at 673 and 7 K. Several additional magnetic contributions to reflections of interplanar spacing values down to $d\sim 1$ Å can be indexed on the basis of a tetragonal cell of lattice constants $a=3.964\,42(3)$ Å and $c=10.5039(2)$ Å with the main magnetic reflections, (111), (113), and (201), marked in the low-temperature pattern of Fig. 3. These magnetic reflections indicate that $^{153}EuMn_2Si_2$ orders in a collinear antiferromagnetic arrangement of ferro-

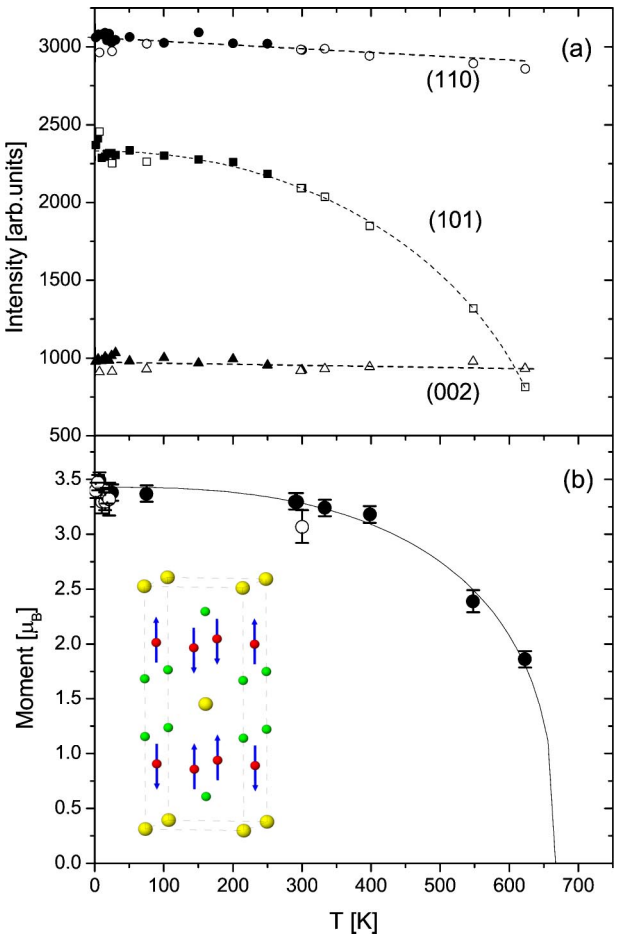

FIG. 2. (a) Graph of the intensity of the (101) superlattice reflection associated with the antiferromagnetic ordering of the Mn sublattice as a function of temperature. Graphs of the variations of the intensities of the nuclear (200) and (110) reflections with temperature are shown for comparison. (b) The variation of the Mn magnetic moment value of $EuMn_2Ge_2$ with temperature. As discussed in the text, the data were fitted to the expression $\mu(T) = \mu(0)[1-(T/T_N)^d]^e$ leading to $T_N = 667(9)$ K and $\mu(0) = 3.43(4)\mu_B$. The full line represents the fit to the data with extrapolation to T_N. The open circles represent the E6 data and the filled circles the GEM data. The axial antiferromagnetic structure of $EuMn_2Ge_2$ below $T_N = 667$ K is also depicted (space group $I4'/m'm'm$).

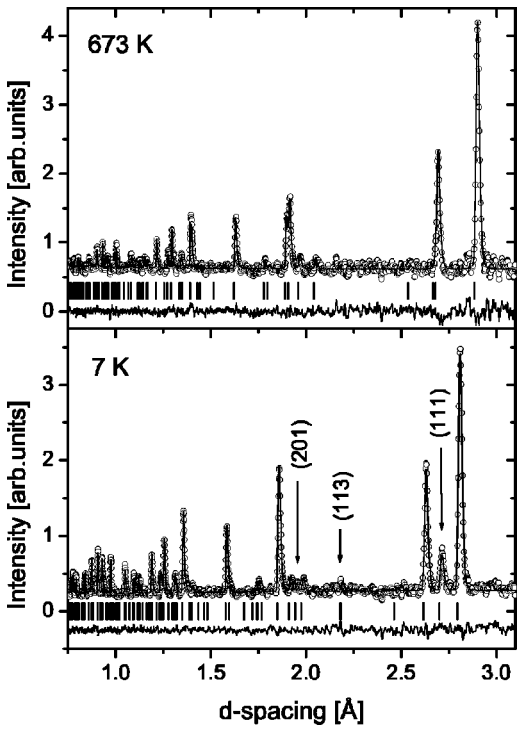

FIG. 3. Rietveld refinements to the time of flight neutron powder diffraction patterns of $^{153}EuMn_2Si_2$ at 673 and 7 K, above and below $T_N = 391(5)$ K, respectively. The (*hkl*) values of the most prominent magnetic reflections are marked in the 7 K pattern, as discussed in the text.

magnetic (001) Mn layers coupled antiferromagnetically along the *c* axis with the Mn moments directed parallel and antiparallel to the *c* axis, as shown in Fig. 4. The magnetic space group of $^{153}EuMn_2Si_2$ is $I_p4/m'm'm'$ and refinement of the pattern at $T \sim 7$ K leads to a moment value of $\mu_{Mn} = 1.97(2)\ \mu_B$. As indicated in Fig. 3, the quality of the fit is good with a χ^2 value of ~2.0. Figure 4 also shows the variation of the Mn magnetic moment values of $EuMn_2Si_2$ (closed symbols) with temperature. An analysis of the moment data to the expression $\mu(T) = \mu(0)[1-(T/T_N)^d]^e$ leads to a Néel temperature $T_N = 391(5)$ K for $^{153}EuMn_2Si_2$. This value is in good agreement with the Néel temperature $T_N = 395$ K, determined by Nowik *et al.*[6] from their magnetization and Mössbauer effect studies of $EuMn_2Si_2$. The present results also show good agreement with the magnetic hyperfine field values determined from their ^{57}Fe Mössbauer studies of $EuMn_2Si_2$ doped with ^{57}Fe. The hyperfine field values were normalized to the moment on the Mn atoms at the common measuring temperature of 150 K [$B_{hf} \sim 12$ T, $\mu_{Mn}(150) = 1.90(2)\ \mu_B$], corresponding to a conversion factor of 6.3 T μ_B^{-1}. On the other hand, no evidence was found in the present experiments for reorientation transitions in $EuMn_2Si_2$ at 107, 65, and 32 K, as reported previously.[6] Based on their magnetization measurements, Nowik *et al.*[6] reported a canting angle with respect to the *c* axis of only 6° at 5 K; should such canting occur, it would correspond to an additional Mn component in the (110) plane of around $\sim 0.2\ \mu_B$, below the detection limit of our neutron diffraction experiments. In summary, $EuMn_2Si_2$ exhibits the collinear antiferromagnetic shown in Fig. 4 below $T_N = 391(5)$ K, with no evidence for reorientation effects on the Mn sublattice, as proposed previously.[6]

It should be noted that the magnetic structures exhibited by $EuMn_2Ge_2$ and $EuMn_2Si_2$ are consistent with the in-plane magnetic coupling expected from their intralayer separation distances, d_{Mn-Mn}. As summarized by Venturini *et al.*,[26] RMn_2Ge_2 and RMn_2Si_2 compounds with $d_{Mn-Mn} < \sim 2.86$ Å have ferromagnetically coupled Mn planes, whereas with $d_{Mn-Mn} > \sim 2.86$ Å, antiferromagnetic or mixed Mn planes are obtained. $EuMn_2Ge_2$ with $d_{Mn-Mn} \sim 3.0$ Å at room temperature exhibits the expected antiferromagnetic coupling within the Mn planes [Fig. 2(b)], whereas

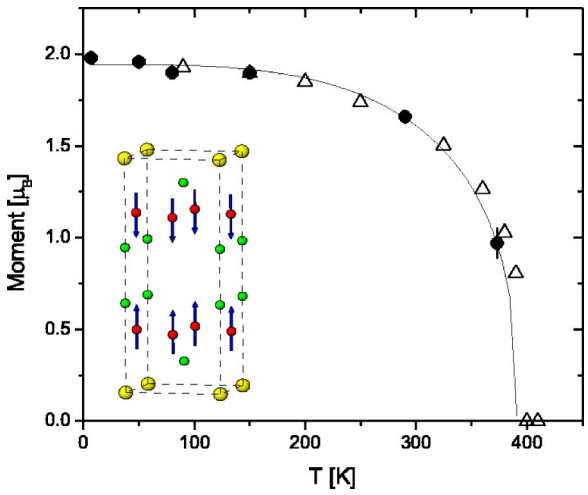

FIG. 4. The variation of the Mn magnetic moment values of $EuMn_2Si_2$ (closed symbols) with temperature. The full line represents the fit to $\mu(T)=\mu(0)[1-(T/T_N)^d]^e$ leading to $T_N=391(5)$ K and $\mu(0)=1.95(2)\ \mu_B$. As discussed in the text the open symbols represent the ^{57}Fe magnetic hyperfine field values of $EuMn_2Si_2$ (Ref. 6) normalized to the value of the Mn moment at 150 K, $\mu_{Mn}(150)=1.90(2)\ \mu_B$. The antiferromagnetic structure of $EuMn_2Si_2$ below $T_N=391$ K with ferromagnetic (001) Mn layers coupled antiferromagnetically along the c axis (space group $I_p4/m'm'm'$) is also depicted.

$EuMn_2Si_2$ with $d_{Mn-Mn}\sim 2.81$ Å at room temperature exhibits ferromagnetic coupling within the Mn planes, as expected (Fig. 4).

C. Valence transition

As explained elsewhere, both the ^{151}Eu and the ^{153}Eu isotopes are suitable for isomer shifts measurements.[1] Consequently, intermediate valence effects in several Eu systems have been investigated by ^{151}Eu Mössbauer studies. In the case of $EuMn_2Si_2$, as shown in Fig. 5(a), the ^{151}Eu isomer shift measurements reveal a valence transition from trivalent Eu for $T<\sim 90$ K to an intermediate valence state for Eu at high temperatures, $T>\sim 600$ K.[6] As discussed below, the valence transition in this $EuMn_2Si_2$ sample is centered around $T_v\sim 496$ K.

Clear evidence for a thermally driven change in the valence state of $EuMn_2Si_2$ is also revealed by the refinements to the present neutron diffraction patterns of $^{153}EuMn_2Si_2$. It has been pointed out that in the $ThCr_2Si_2$-type structure, the a lattice parameter is largely determined by the size of the rare earth ion, while the c lattice parameter depends upon the transition metal–silicon distances. However, in Eu-based compounds with the $ThCr_2Si_2$-type structure, it is not uncommon that both lattice parameters are determined by the Eu valence [e.g., in the $EuNi_2(Si_{1-x}Ge_x)_2$ series[27]]. In the current $^{153}EuMn_2Si_2$ studies, the a and c lattice parameters are found to show similar changes with temperature [Fig. 5(a)], with the unit cell volume of $^{153}EuMn_2Si_2$ increasing by ~7% from 300 to 723 K [Fig. 5(b)]. We have applied the interconfigurational fluctuation (ICF) model[14,15] to the analysis of the volume changes resulting from the

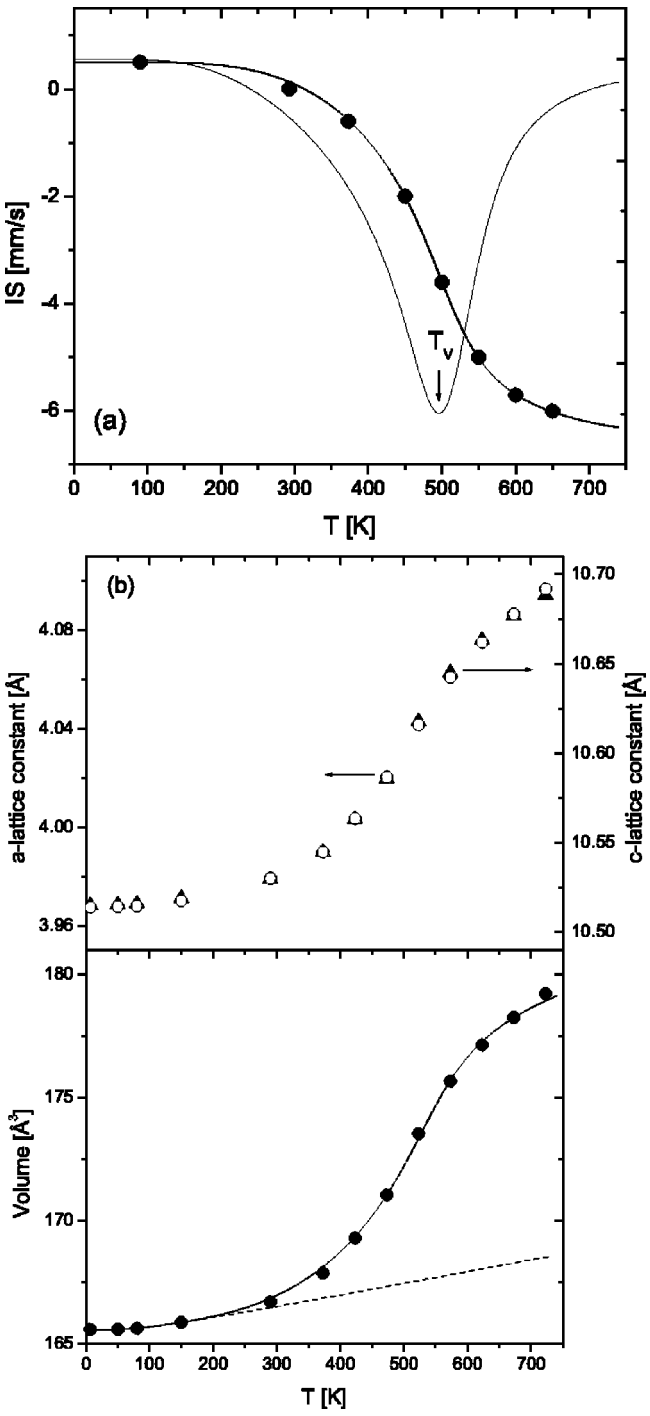

FIG. 5. (a) The ^{151}Eu isomer shift of $EuMn_2Si_2$ (closed symbols, Ref. 6) with the full line representing our fit to the data using the ICF model (Ref. 15). Also shown is the derivative of the ICF fit to the isomer shift data, leading to a valence transition temperature of $T_v\sim 496$ K. (b) The a lattice parameter (○; left scale) and the c lattice parameter (▲; right scale) of $^{153}EuMn_2Si_2$ along with the unit cell volume (●) as a function of temperature. The dashed line shows the lattice expansion derived from a fit to the low-temperature data ($T<150$ K) based on the Einstein model as described in the text.

temperature-induced valence transition in a concentrated Eu compound for the first time. This extension of the ICF model to include the effects of cooperative phenomena has also been used successfully to account for the temperature-induced valence transition in $EuPd_2Si_2$, as monitored by ^{151}Eu isomer shift measurements,[15] and the temperature and field-induced valence transitions in $Eu(Pd_{1-x}Pt_x)_2Si_2$[7] and $EuNi_2(Si_{1-x}Ge_x)_2$ as monitored by magnetic susceptibility and high field magnetization measurements.[8]

In the ICF model, the rare earth ions are described as fluctuating in time between two configurations, with each configuration being characterized by a different integral occupation of the $4f$ shell. Assuming a Eu^{3+} ground state, the ratio of the occupation probabilities of the Eu^{2+} and Eu^{3+} states, represented by p_2 and p_3, respectively, is given by

$$\frac{p_2}{p_3} = \frac{8\exp[-E_{ex}/kT^*]}{1+3\exp[-480/T^*]+5\exp[-1330/T^*]+\cdots}, \quad (1)$$

where $p_2+p_3=1$, 480 and 1330 K are the energies of the first ($J=1$) and second ($J=2$) excited spin–orbit states of the Eu^{3+} configuration and E_{ex} is the excitation energy required to convert an Eu^{3+} configuration into an Eu^{2+} configuration. $T^*=\sqrt{T^2+T_F^2}$ takes account of the energy level broadening (of magnitude T_f) due to hybridization.[15] The relatively sharp transitions exhibited by both the isomer shift and the volume data indicate that cooperative interactions take place among the Eu charge fluctuations in this concentrated Eu compound. The data were therefore analyzed, assuming that the excitation energy, E_{ex}, depends on the probability for the valence state p_2 as $E_{ex}=E_0(1-\alpha p_2)$, where E_0 represents the average excitation energy at $T=0$ K for all atoms and α is the average interaction parameter.[15] An important aspect of our analysis is a separation of the normal lattice expansion from the measured unit cell volume in order to isolate the valence-induced changes. The dashed line in Fig. 5(b) represents the lattice expansion fit for data up to $T\sim150$ K using an Einstein expression of the form $V(T)=V_0+K_E/(\exp(T_E/T)\text{-}1)$, where T is the temperature, K_E is the Einstein constant, and T_E is an effective Einstein temperature.[28] The Einstein model was chosen as a convenient method of describing accurately the volume expansion data and leads to the fit parameters: $V(0)=165.578(6)$ Å^3; $T_E=249(35)$ K and $K_E=1.2(3)$ Å^3. The net volume change, $\Delta V_{val}(T)$, due to the thermally driven valence change can be expressed in terms of $\Delta V=(V^{2+}-V^{3+})$, the difference in volume between the Eu^{2+} and Eu^{3+} configurations, as $\Delta V_{val}(T)=p_2\,\Delta V$, where p_2 is defined in Eq. (1). The optimal fit to the valence-induced volume changes [Fig. 6(a)] leads to $E_0=1656(2)$ K, $T_F=56(2)$ K, and $\alpha=1.09(1)$ with a fitted value for the difference in volume between the Eu^{2+} and Eu^{3+} configurations of $\Delta V=18.18(5)$ Å^3. The derivative of the ICF fit to the volume data shown in Fig. 6(a) leads to a valence transition temperature of $T_v\sim527$ K for the present $^{153}EuMn_2Si_2$ sample with a full width at half-maximum for the derivative curve of $\Delta T\sim150$ K. The asymmetry in this latter curve demonstrates that the valence transition proceeds more rapidly with increasing temperature, as expected. The variation of $p_2^{\Delta V}(T)$, the occupation probability of the Eu^{2+} state resulting from these volume changes with temperature, along with the average valence values, Eu^{val}, for the thermally driven valence transition in $^{153}EuMn_2Si_2$, are shown as full lines in Fig. 6(b).

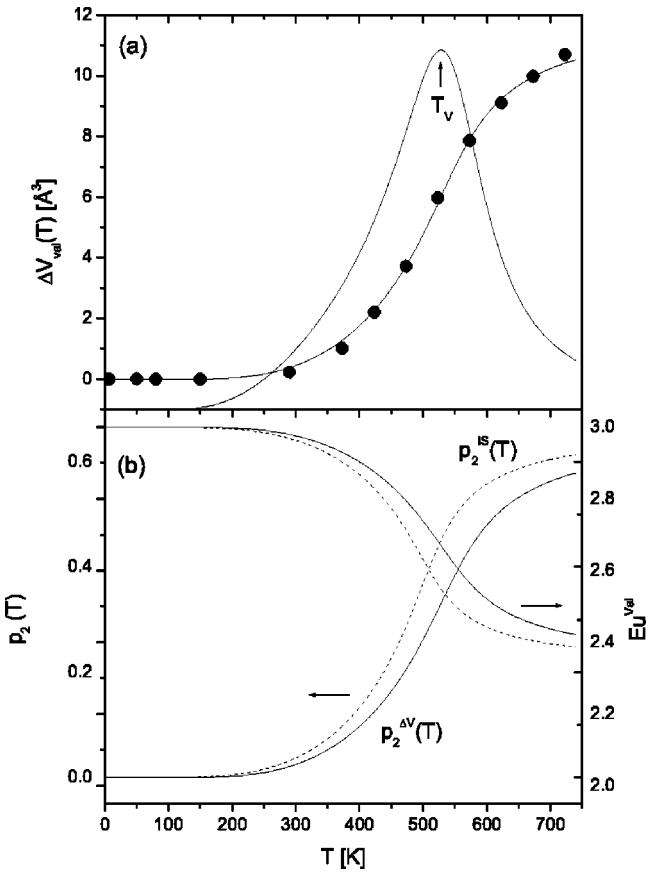

FIG. 6. (a). The valence-induced volume changes in $^{153}EuMn_2Si_2$ as a function of temperature, with the full line representing our fit to the data using the ICF model,[15] as described in the text. The derivative of the ICF fit to the volume data due is also shown, leading to a valence transition temperature of $T_v\sim527$ K. (b) The variation of $p_2^{\Delta V}(T)$, the occupation probability of the Eu^{2+} state resulting from the volume changes (full line; left scale) along with the average valence values, Eu^{val} (full line; right scale) for the thermally driven valence transition in $^{153}EuMn_2Si_2$. The equivalent $p_2^{IS}(T)$ and Eu^{val} values (dashed lines) derived from the fit to the Mössbauer isomer shift data of Fig. 5(a) are also shown.

The full line through the data in Fig. 5(a) shows our analysis of the ^{151}Eu isomer shift data (the isomer shift values of $Eu^{3+}=0.5$ mm/s and $Eu^{2+}=-10.1$ mm/s were taken from the data of $^{151}EuMn_2Si_2$ and $^{151}EuMn_2Ge_2$, respectively[6]). This leads to the fit parameters of $E_0=1600(10)$ K; $T_f=104(2)$ K; $\alpha=1.12(2)$ (by comparison, Nowik *et al.*[6] derived the values $E_0=1610$ K and $\alpha=1.35$, T_f value not given, in their analysis of the isomer shift data). The derivative of the present ICF fit to the isomer shift data [Fig. 5(a)] leads to $T_v\sim496$ K, similar to the value $T_v\sim527$ K determined for the present $^{153}EuMn_2Si_2$ sample. As is evident from Fig. 6(b), the $p_2(T)$ and average Eu^{val} values

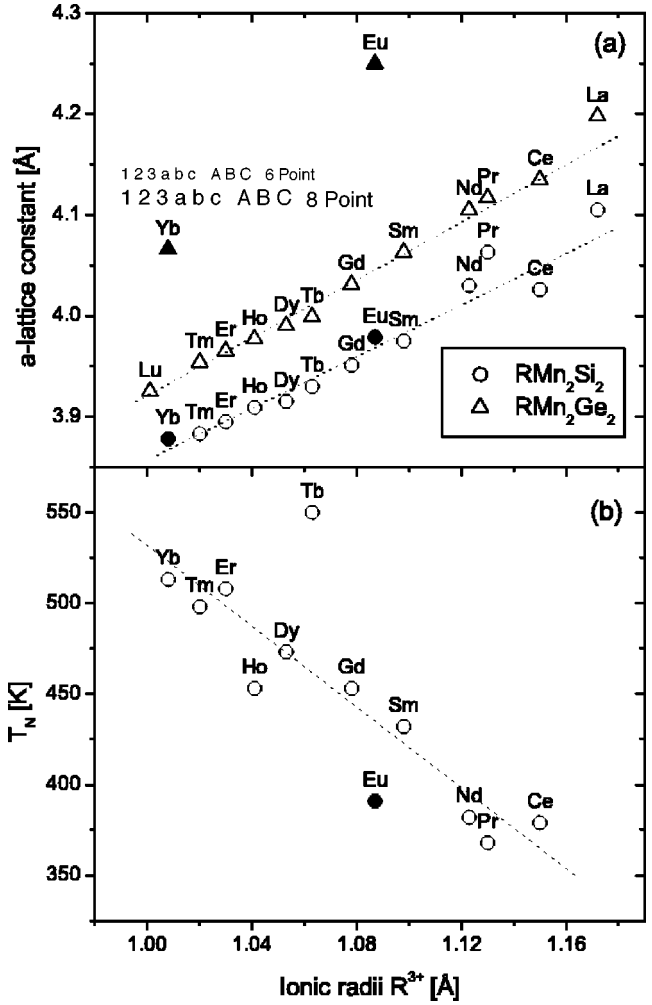

FIG. 7. (a) Values of the *a* lattice parameters of the RMn_2Si_2 and RMn_2Ge_2 series at room temperature as a function of the R^{3+} ionic radii.[21] The lattice parameters values for the Eu compounds are derived from the current measurements, the Yb data from,[28] with the other data taken from.[4] (b) The Néel temperatures of RMn_2Si_2 intermetallic compounds derived from the literature, e.g., Refs. 14, 19, as a function of the R^{3+} ionic radii. The dashed line shows the trend of the average Néel temperatures for the RMn_2Si_2 series, as discussed in the text.

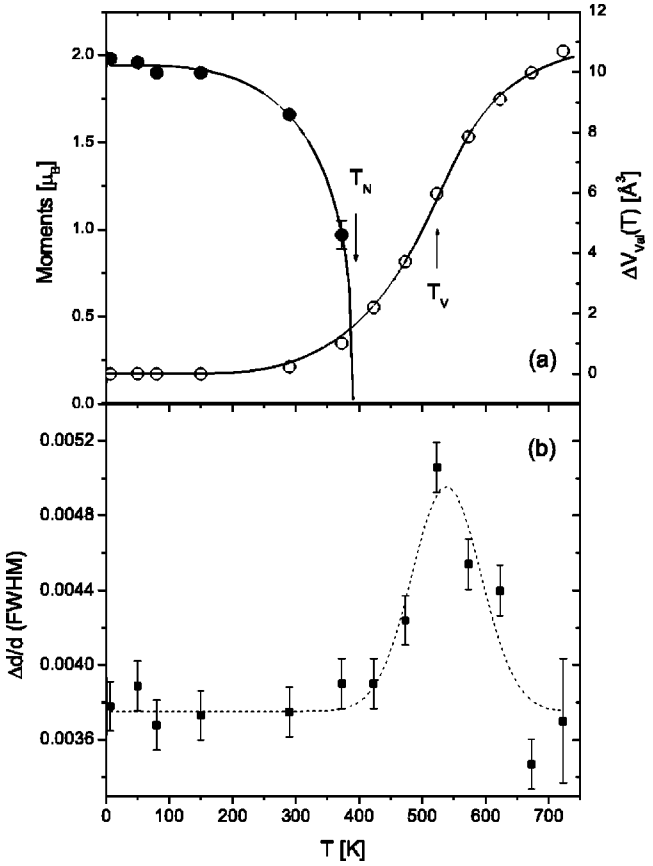

FIG. 8. (a) Graphs of the Mn magnetic moment (cf. Fig. 4) and the valence-induced volume change [Fig. 6(a)] of $EuMn_2Si_2$ as a function of temperature. (b) The variation of the linewidth of the (110) reflection (expressed in terms of the interplanar spacing *d*) of $EuMn_2Si_2$ as a function of temperature. The dashed line shows a Gaussian fit to the data to act as a guide for the eye.

determined from changes in the volume (full lines) and isomer shift (dashed lines) show good agreement for the thermally driven valence transition in $EuMn_2Si_2$.

Figure 7(a) shows a comparison of the *a* lattice parameters for $EuMn_2Si_2$ and $EuMn_2Ge_2$ at room temperature with the *a* parameters for other compounds in the RMn_2Si_2 and RMn_2Ge_2 series as a function of the R^{3+} ionic radii given in Ref. 21. These results allow the predominant difference in the Eu valence states of $EuMn_2Si_2$ and $EuMn_2Ge_2$ to be distinguished. In particular, the trends of the RMn_2Si_2 data demonstrate that $EuMn_2Si_2$ is consistent with a predominantly trivalent-like behavior of the Eu ion at room temperature, whereas the significant deviation for $EuMn_2Ge_2$ from the trend of the lattice parameter data for RMn_2Ge_2 reflects a nontrivalent Eu state. As noted above, given that the dimensions of the basal plane in this tetragonal $ThCr_2Si_2$-type structure are determined predominantly by the radii of the rare earth atoms, this deviation in the *a* lattice parameter provides strong evidence for a change in the valence state of Eu from the predominant trivalent-like behavior of $EuMn_2Si_2$ at room temperature to a mixed valence or even divalent state in $EuMn_2Ge_2$. In a similar manner, the relatively large cell parameters of $YbMn_2Ge_2$ [Fig. 7(a)] indicates a larger Yb radius than that expected of a trivalent Yb ion, with an analysis leading to a Yb valence state of about 2.35 in $YbMn_2Ge_2$ at room temperature.[29]

As is evident in Fig. 7(b), $EuMn_2Si_2$ exhibits a relatively low value for its antiferromagnetic ordering temperature, $T_N = 391$ K, compared with the Néel temperatures exhibited by the trend of neighboring RMn_2Si_2 compounds. Further support for this indication that the magnetic transition in $EuMn_2Si_2$ is inhibited by the valence change is provided by Fig. 8(a), which shows the temperature evolution of both the Mn magnetic moment (data reproduced from Fig. 4) and the valence-induced volume change [Fig. 6(a)]. Given the excess volume associated with the valence transition and the reduced valence state of $EuMn_2Si_2$ at high temperatures, as discussed above [Fig. 5(b)], this excess volume is caused by the changing electronic configuration [cf. e.g., Fig. 6(b)],

which, in turn, inhibits the magnetic ordering of the Mn sublattice. The Néel temperature of $EuMn_2Si_2$ appears to have been reduced by ~10%–15% compared to the value of ~450 K derived from the extrapolation of T_N for the neighboring rare earth intermetallics. This correspondingly indicates that the exchange interaction parameter in $EuMn_2Si_2$ is reduced by ~10%–15% as a result of the valence change. The correlation between the loss of antiferromagnetic order and the onset of the volume changes around T_N—as is evident in Fig. 8(a)—indicates that the magnetic transition is probably initiated by changes in the conduction band structure caused by the drastic changes in the Eu valence. Further evidence of the structural changes occurring in $EuMn_2Si_2$ as a result of the thermally driven valence transition is provided by Fig. 8(b), which shows the variation of the linewidth of the (110) reflection as a function of temperature. Here the peak in linewidth occurs around $T_v \sim 527$ K, reflecting the significant lattice strains present in $EuMn_2Si_2$ as the valence transition occurs.

IV. CONCLUSIONS

The magnetic structures of $EuMn_2Ge_2$ and $EuMn_2Si_2$ have been determined by neutron diffraction measurements (~1.8–723 K) on samples prepared with the low neutron absorption isotope ^{153}Eu. The Mn sublattice of $EuMn_2Ge_2$ has magnetic moments pointing in opposite directions along the *c* axis below a Néel temperature of $T_N = 667(9)$ K [Fig. 2(b); space group $I4'/m'm'm$]. $EuMn_2Si_2$ also displays collinear antiferromagnetism below its ordering temperature of $T_N = 391(5)$ K with ferromagnetically coupled (001) Mn layers coupled antiferromagnetically along the *c* axis and the Mn moments directed parallel and antiparallel to the *c* axis (Fig. 4; space group $I_p4/m'm'm'$). Contrary to the findings of magnetization measurements,[6] there is no evidence for ordering of the Eu^{+2} ions in $EuMn_2Ge_2$ down to 1.5 K.

The valence-driven volume changes in $EuMn_2Si_2$ [Fig. 6(a)] have been analyzed for the first time in terms of the interconfigurational fluctuation model, extended in order to take the effect of cooperative phenomena into account.[14,15] This leads to a valence transition temperature of $T_v \sim 527$ K and occupation probabilities, $p_2^{\Delta V}(T)$, for the Eu^{2+} state, in good agreement with the $p_2^{IS}(T)$, curve determined from our reanalysis of earlier $^{151}EuMn_2Si_2$ isomer shift data [Fig. 6(b)]. The average Eu^{val} values determined from the volume and isomer shift changes are also in good agreement [Fig. 6(b)], thus demonstrating the applicability of the interconfigurational fluctuation model in enabling valence changes induced by volume changes in Eu and related compounds to be determined. The change in the electronic configuration of $EuMn_2Si_2$ resulting from the thermally induced valence transition reduces the magnetic interaction parameter for antiferromagnetic ordering of the Mn sublattice by ~10%–15%.

ACKNOWLEDGMENTS

SJC acknowledges renewal of his Alexander von Humboldt Research Fellowship during his stay at the Technische Universität München. SJC also acknowledges support from Access to the Major Research Facilities Program, Australian Nuclear Science and Technology Organization. This project is supported in part by the award of a Discovery Grant from the Australian Research Council. We thank BENSC, Hahn-Meitner-Institut, Berlin for access to the E6 diffractometer.

*Former address: Rutherford Appleton Laboratory, ISIS, Didcot, OX11 0QX, United Kingdom. Electronic mail: michael.hofmann@frm2.tum.de

[1] I. Nowik, Hyperfine Interact. **13**, 89 (1983).
[2] P. Wachter, in *Handbook of the Physics and Chemistry of Rare Earths*, edited by K. A. Gschneider, Jr., L. Leyring, G. H. Lander, and G. R. Choppin (Elsevier, Amsterdam, 1994).
[3] *Proceedings of the International Conference on Strongly Correlated Electron Systems*, SCES2002 (July 2002, Cracow, Poland), Acta Physics Polonica B **34** (2003).
[4] A. Szytula and J. Leciejewicz, *Handbook of Crystal Structures and Magnetic Properties of Rare Earth Intermetallics* (CRC Press, Boca Raton, 1994).
[5] G. Wortmann, I. Nowik, B. Perscheid, G. Kaindl, and I. Felner, Phys. Rev. B **43**, 5261 (1991).
[6] I. Nowik, I. Felner, and E. R. Bauminger, Phys. Rev. B **55**, 3033 (1997).
[7] I. A. Mitsuda, H. Wada, M. Shiga, H. Aruga Kutori, and T. Goto, Phys. Rev. B **55**, 12474 (1997).
[8] H. Wada, A. Nakamura, A. Mitsuda, M. Shiga, T. Tanaka, H. Mitamur, and T. Goto, J. Phys.: Condens. Matter **9**, 7913 (1997).
[9] G. Venturini, R. Welter, E. Ressouche, and B. Malaman, J. Magn. Magn. Mater. **150**, 197 (1995).
[10] E. V. Sampathkumaran, L. C. Gupta, R. Vijayayghavan, K. V. Gopalakrishnan, R. G. Pillay, and H. G. Devare, J. Phys. C **14**, L237 (1981).
[11] M. M. Abd-Elmeguid, C. H. Sauer, and W. Zinn, Phys. Rev. Lett. **55**, 2467 (1985).
[12] H. J. Hesse and G. Wortmann, Hyperfine Interact. **93**, 1499 (1994).
[13] R. Welter and B. Malaman, J. Alloys Compd. **354**, 35 (2003).
[14] B. C. Sales and D. K. Wohlleben, Phys. Rev. Lett. **35**, 1240 (1975).
[15] M. Croft, J. A. Hodges, E. Kemly, A. Krishan, V. Nurgai, and L. C. Gupta, Phys. Rev. Lett. **48**, 826 (1982).
[16] A. C. Larson and R. B. Von Dreele, ''General structure analysis system (GSAS),'' Los Alamos National Laboratory Report LAUR 86-748, 2000.
[17] W. G. Williams, R. M. Ibberson, P. Day, and J. E. Enderby, Physica B **241–243**, 234 (1998).
[18] M. Hofmann, S. J. Campbell, S. J. Kennedy, and X. L. Zhao, J. Magn. Magn. Mater. **176**, 279 (1997).
[19] B. Malaman, G. Venturini, R. Welter, and E. Ressouche, J. Alloys Compd. **210**, 209 (1994).
[20] W. Dorrscheidt, N. Niess, and H. Schafer, Z. Naturforsch. B **31**, 890 (1976).
[21] R. D. Shannon, Acta Crystallogr., Sect. A: Cryst. Phys., Diffr., Theor. Gen. Crystallogr. **32**, 751 (1976).
[22] I. Felner and I. Nowik, J. Phys. Chem. Solids **39**, 763 (1978).
[23] K. Hagdorn, D. Hohlwein, J. Ihringer, K. Knorr, W. Prandl, H. Ritter, H. Schmid, and Th. Zeiske, Eur. J. Biochem. **11**, 243 (1999).

[24] R. Welter, G. Venturini, and B. Malaman, J. Alloys Compd. **206**, 55 (1994).
[25] B. T. Matthias, R. M. Bozorth, and J. H. Van Vleck, Phys. Rev. Lett. **7**, 160 (1961).
[26] G. Venturini, R. Welter, E. Ressouche, and B. Malaman, J. Alloys Compd. **223**, 101 (1995).
[27] H. Wada, T. Sakata, A. Nakamura, A. Mitsuda, M. Shiga, Y. Ikeda, and Y. Bando, J. Phys. Soc. Jpn. **68**, 950 (1999).
[28] K. S. Knight, I. C. Stretton, and P. F. Schofield, Phys. Chem. Miner. **26**, 477 (1999).
[29] M. Hofmann, S. J. Campbell, and A. V. J. Edge, Appl. Phys. A: Mater. Sci. Process. **74**, 1233 (2002).